
This is an electronic reprint of the original article.
This reprint may differ from the original in pagination and typographic detail.

Koppinen, Jussi; Kukkola, Jarno; Hinkkanen, Marko

Parameter estimation of an LCL filter for control of grid converters

Published in:

9th International Conference on Power Electronics (ICPE 2015-ECCE Asia)

DOI:

[10.1109/ICPE.2015.7167942](https://doi.org/10.1109/ICPE.2015.7167942)

Published: 01/06/2015

Document Version

Peer-reviewed accepted author manuscript, also known as Final accepted manuscript or Post-print

Please cite the original version:

Koppinen, J., Kukkola, J., & Hinkkanen, M. (2015). Parameter estimation of an LCL filter for control of grid converters. In *9th International Conference on Power Electronics (ICPE 2015-ECCE Asia)* (pp. 1260-1267). <https://doi.org/10.1109/ICPE.2015.7167942>

This material is protected by copyright and other intellectual property rights, and duplication or sale of all or part of any of the repository collections is not permitted, except that material may be duplicated by you for your research use or educational purposes in electronic or print form. You must obtain permission for any other use. Electronic or print copies may not be offered, whether for sale or otherwise to anyone who is not an authorised user.

Parameter Estimation of an LCL Filter for Control of Grid Converters

Jussi Koppinen, Jarno Kukkola, and Marko Hinkkanen

Aalto University School of Electrical Engineering

P.O. Box 13000, FI-00076 Aalto, Helsinki, Finland

Abstract—Model-based control techniques are frequently used with grid-connected converters. This paper proposes a method for identifying model parameters of an LCL filter connected to a grid converter for control purposes. In identification, a discrete-time autoregressive moving average with exogenous input (ARMAX) model structure is used and closed-loop current control is considered. The resulting discrete-time model parameters are translated into the continuous-time physical parameters (inductance and capacitance values of the filter) by comparing the estimated discrete-time model with the analytical discrete-time model. Simulation and experimental results show that the proposed method yields good parameter estimates that are suitable for control tuning.

Index Terms—Identification, LCL filter, physical parameters, self commissioning.

I. INTRODUCTION

LCL filters are increasingly used in connection with grid-connected converters due to their effective attenuation of switching harmonics. The resonance caused by the LCL filters makes control of these converters more challenging. The resonance should be damped sufficiently, preferably with active methods, so that additional losses can be avoided. In order to apply model-based control techniques in converter control or active damping the parameters of the LCL-filter model must be known [1]–[3].

Fig. 1 shows a space-vector model of the lossless LCL filter. If the model parameters (inductance and capacitance values) are unknown, they could be either measured or estimated. The estimation methods are usually preferred, since the measuring methods require additional equipment. Generally, the estimation methods can be divided into two subclasses: nonparametric and parametric estimation methods [4]. The nonparametric methods estimate the frequency response of a system while the parametric methods estimate parameters from a predefined model structure. From control point of view, the parametric methods are more interesting since the parameters can be used in control tuning.

Various methods have been proposed for estimating the grid impedance [5]–[14], the converter-side impedance [15], and the DC-side capacitance [16]. However, only a small number of studies have considered the whole LCL filter [17], [18]. Further, adaptive control methods have been proposed for the grid converters, taking into account the variation of the grid inductance [19], [20] and the grid frequency [21].

In [5], the grid impedance is measured using sinusoidal current signal injection. However, additional equipment is

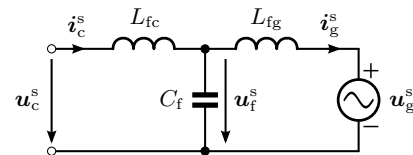


Fig. 1. Space-vector circuit model of the LCL filter connected to the inductive grid in stationary coordinates (denoted by the superscript s).

required and the procedure takes several minutes to complete. In [6], the grid inductance is estimated using the knowledge of the LCL-filter resonance frequency. However, the method [6] requires a look-up table in which the relationship between the resonance frequency and the LCL-filter parameters is precalculated in various situations if the ratio between the converter-side inductance and the grid-side inductance is less than ten. In practical LCL-filter designs, the ratio between the converter-side inductance and the grid-side inductance can be less than ten [22]. In [7], an extended Kalman filter (EKF) is used to estimate the inductive and resistive parts of the grid impedance. However, perhaps the most serious disadvantage of this method is that the tuning of the covariance matrices of the EKF is based on a trial-and-error procedure. In [8], the estimated grid impedance is used for active islanding detection.

In [14], the frequency response of an LC circuit is measured using a pseudo-random binary sequence (PRBS) as the excitation signal which enables fast estimation procedure. In [10], the grid inductance is solved from the estimated LC-circuit frequency response excited by an impulse signal. Both methods [10] and [14] require a high sampling frequency as well as measurements of the capacitor voltages and converter-side currents. In [19], an adaptive state-feedback controller is proposed for a grid converter with an LCL filter. However, the LCL-filter parameters are assumed to be known in initialization. In [17], a discrete-time state-space model of the LCL filter is estimated in open loop. However, the method does not provide the physical parameters of the LCL filter.

In this paper, we propose a method for estimating the physical parameters (the two inductances and the capacitance) of the LCL filter by comparing the estimated discrete-time model with an analytical discrete-time model. The PRBS is used as an excitation signal and injected into the reference voltage of the converter. In identification, a discrete-time autoregressive moving average with exogenous input (ARMAX)

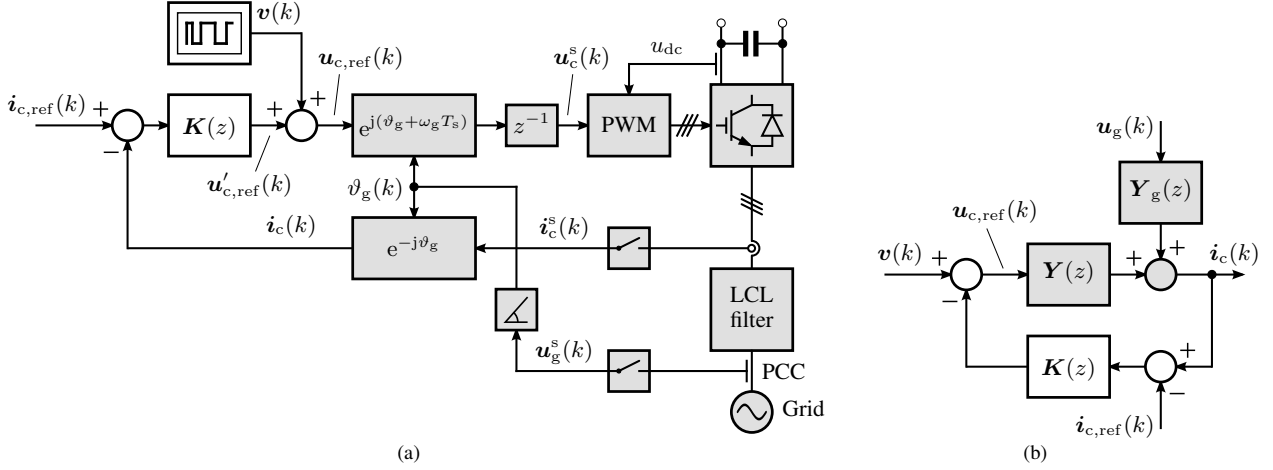


Fig. 2. (a) Grid-converter system during identification. Sampling of the measured signals and the computational delay z^{-1} are shown. The sampling of the converter currents and the grid voltages is synchronized with the PWM. The effect of the computational delay z^{-1} on the angle of the converter voltage \mathbf{u}_c^s is compensated for in the coordinate transformation. The DC-link voltage u_{dc} is measured for the PWM, which calculates the duty cycles for the power switches. The grid-voltage angle ϑ_g is calculated from the measured grid voltages using a phase-locked loop (PLL). (b) Equivalent block diagram from the controller point of view. In both subfigures, the gray blocks represent the plant model.

model structure is used. Identification is performed using the indirect method [23], i.e., the effect of the current controller is taken into account. The proposed method: 1) requires neither an injection circuit nor additional sensors; 2) provides the desired parameters of the lossless LCL-filter model needed in the controller [3]; and 3) gives insight into the physical system due to obtained physical parameters [24].

II. SYSTEM MODEL

A. Continuous-Time Model

The LCL filter is modeled as the converter-side inductance L_{fc} , the capacitance C_f , and the grid-side inductance L_{fg} as shown in Fig. 1. The grid-voltage vector is denoted by \mathbf{u}_g . Complex-valued space vectors and switching-cycle averaged quantities are used. In synchronous coordinates rotating at the grid angular frequency ω_g , the converter current \mathbf{i}_c can be expressed as

$$\mathbf{i}_c = \mathbf{Y}'(s)\mathbf{u}_c + \mathbf{Y}'_g(s)\mathbf{u}_g \quad (1)$$

where the transfer operators $\mathbf{Y}'(s)$ and $\mathbf{Y}'_g(s)$ are marked with the prime in order to separate them from their discrete-time counterparts. The transfer operator from the converter voltage \mathbf{u}_c to the converter current \mathbf{i}_c is

$$\mathbf{Y}'(s) = \frac{1}{(s + j\omega_g)L_{fc} + (s + j\omega_g)^2 + \omega_z^2} \quad (2)$$

where

$$\omega_p = \sqrt{\frac{L_{fc} + L_{fg}}{L_{fc}L_{fg}C_f}} \quad \text{and} \quad \omega_z = \sqrt{\frac{1}{L_{fg}C_f}} \quad (3)$$

are the resonance frequency and the anti-resonance frequency of the filter, respectively. The transfer operator $\mathbf{Y}'_g(s)$ from the grid voltage \mathbf{u}_g to the converter current \mathbf{i}_c could be easily derived from Fig. 1.

B. Hold-Equivalent Discrete-Time Model

Fig. 2(a) shows the block diagram of the grid-converter system equipped with the LCL filter. A discrete-time model of the lossless LCL filter in synchronous coordinates is presented in the following (cf. Appendix A). In the derivation of the model, the pulse-width modulator (PWM) is modeled as the zero-order hold (ZOH) in stationary coordinates. The sampling synchronized to the ZOH is assumed. Further, the one-sampling-period time delay z^{-1} due to the finite computation time of the digital control system is included in the model. Under these assumptions, the converter current $\mathbf{i}_c(k)$ depends on the converter voltage reference $\mathbf{u}_{c,\text{ref}}(k)$ and the grid voltage $\mathbf{u}_g(k)$ according to

$$\mathbf{i}_c(k) = \mathbf{Y}(z)\mathbf{u}_{c,\text{ref}}(k) + \mathbf{Y}_g(z)\mathbf{u}_g(k) \quad (4)$$

where k is the discrete-time index, z is the forward shift operator, and $\mathbf{Y}_g(z)$ is the pulse-transfer operator from the grid voltage $\mathbf{u}_g(k)$ to the converter current $\mathbf{i}_c(k)$. The pulse-transfer operator from the voltage reference $\mathbf{u}_{c,\text{ref}}(k)$ to the converter current $\mathbf{i}_c(k)$ can be expressed as

$$\mathbf{Y}(z) = z^{-1} \frac{\beta_1 \gamma z^{-1} + \beta_2 \gamma^2 z^{-2} + \beta_1 \gamma^3 z^{-3}}{1 + \alpha_1 \gamma z^{-1} - \alpha_1 \gamma^2 z^{-2} + \gamma^3 z^{-3}} \quad (5)$$

where $\gamma = e^{-j\omega_g T_s}$ and T_s is the sampling period. The parameters are

$$\begin{aligned} \alpha_1 &= -1 - 2 \cos(\omega_p T_s) \\ \beta_1 &= \frac{1}{L_t} \left(T_s + \frac{L_{fg} \sin(\omega_p T_s)}{\omega_p L_{fc}} \right) \\ \beta_2 &= -\frac{2}{L_t} \left(T_s \cos(\omega_p T_s) + \frac{L_{fg} \sin(\omega_p T_s)}{\omega_p L_{fc}} \right) \end{aligned} \quad (6)$$

where $L_t = L_{fc} + L_{fg}$ is the total inductance.

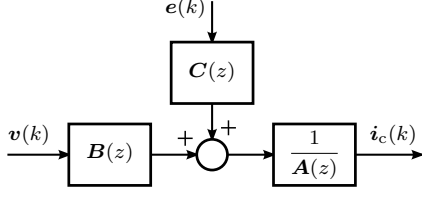


Fig. 3. ARMAX model structure.

III. IDENTIFICATION PROCEDURE

As shown in Fig. 2(a), the current controller $\mathbf{K}(z)$ operates in synchronous coordinates, whose d-axis is fixed to the measured grid voltage, i.e., $\mathbf{u}_g = u_g + j0$. The current reference is $\mathbf{i}_{c,\text{ref}} = i_{cd,\text{ref}} + j i_{cq,\text{ref}}$, where $i_{cd,\text{ref}}$ is the output of the DC-voltage controller and $i_{cq,\text{ref}}$ determines the reactive power.

A. Closed-Loop Identification

The PRBS vector \mathbf{v} is superimposed on the voltage reference $\mathbf{u}'_{c,\text{ref}}$ obtained from the current controller, i.e., $\mathbf{u}_{c,\text{ref}} = \mathbf{u}'_{c,\text{ref}} + \mathbf{v}$. The PRBS has many desirable properties for identification including the wide power spectrum and the lowest possible peak factor [4]. It can be implemented using feedback shift register circuits comprising a deterministic and repeatable signal. The PRBS can have only two possible values (e.g., -1 and 1). The duration of the PRBS is $(2^m - 1)T_s$, where m is the number of shift registers. The duration should be longer than the rise time of the system. The direction of the PRBS vector \mathbf{v} can be chosen perpendicular to the direction of $\mathbf{u}'_{c,\text{ref}}$ in order to minimize the maximum amplitude of $\mathbf{u}_{c,\text{ref}}$ and to reduce the risk of the converter-voltage saturation.

Closed-loop identification could either be performed using a direct method or an indirect method [23]. In this paper, the closed-loop identification is performed using an indirect method, i.e., the effect of the current controller on the regressors is taken into account. In this way, the correlation between the identification input and noise signal can be avoided, and less biased parameter estimates are obtained. From Fig. 2(b), the pulse-transfer operator from $\mathbf{v}(k)$ to $\mathbf{i}_c(k)$ can be solved, resulting

$$\mathbf{i}_c(k) = \frac{\mathbf{Y}(z)}{1 + \mathbf{K}(z)\mathbf{Y}(z)}\mathbf{v}(k) = \frac{\mathbf{B}(z)}{\mathbf{A}(z)}\mathbf{v}(k) \quad (7)$$

For simplicity, the proportional current controller is assumed to be used during identification,

$$\mathbf{K}(z) = k_p \quad (8)$$

where k_p is the (known) gain. Hence, the polynomials in (7) become

$$\begin{aligned} \mathbf{A}(z) &= 1 + \alpha_1 \gamma z^{-1} + (\beta_1 k_p \gamma - \alpha_1 \gamma^2) z^{-2} \\ &\quad + (\gamma^3 + \beta_2 k_p \gamma^2) z^{-3} + \beta_1 k_p \gamma^3 z^{-4} \\ \mathbf{B}(z) &= \beta_1 \gamma z^{-2} + \beta_2 \gamma^2 z^{-3} + \beta_1 \gamma^3 z^{-4} \end{aligned} \quad (9)$$

B. Model Structure

The selection of a model structure is essential for successful identification. A discrete-time ARMAX model structure shown in Fig. 3 is considered [4]. This structure gives enough freedom to describe the properties of the disturbances affecting the converter current. The system (7) is augmented with the noise polynomial $C(z)$, giving

$$\mathbf{A}(z)\mathbf{i}_c(k) = \mathbf{B}(z)\mathbf{v}(k) + C(z)\mathbf{e}(k) \quad (10)$$

where \mathbf{e} is the Gaussian noise component. The second-order noise polynomial

$$C(z) = 1 + c_1 z^{-1} + c_2 z^{-2} \quad (11)$$

is chosen.

In order to be able to estimate the parameters α_1 , β_1 , and β_2 effectively, the system (10) is reformulated in such a way that all known linear dependencies are taken into account, leading to the minimal realization

$$\mathbf{y}(k) = \alpha_1 \varphi_{\alpha 1}(k) + \beta_1 \varphi_{\beta 1}(k) + \beta_2 \varphi_{\beta 2}(k) + C(z)\mathbf{e}(k) \quad (12)$$

where the regressed variable is

$$\mathbf{y}(k) = (1 - \gamma^3 z^{-3})\mathbf{i}_c(k) \quad (13)$$

and the regressors are

$$\begin{aligned} \varphi_{\alpha 1}(k) &= (\gamma^2 z^{-2} - \gamma z^{-1})\mathbf{i}_c(k) \\ \varphi_{\beta 1}(k) &= (\gamma z^{-2} + \gamma^3 z^{-4})[\mathbf{v}(k) - k_p \mathbf{i}_c(k)] \\ \varphi_{\beta 2}(k) &= \gamma^2 z^{-3}[\mathbf{v}(k) - k_p \mathbf{i}_c(k)] \end{aligned} \quad (14)$$

C. Data Acquisition and Preprocessing

The DC components are removed from the samples in order to improve the accuracy of the estimated models [4]. The output and the regressors are constructed at each time step according to (13) and (14) using the measured values of the converter current $\mathbf{i}_c(k)$ and the PRBS $\mathbf{v}(k)$. The output samples are packed into the vector

$$\mathbf{Y} = [\mathbf{y}(5) \quad \mathbf{y}(6) \quad \dots \quad \mathbf{y}(N)]^T \quad (15)$$

where N is the number of samples used in the algorithm. Similarly, the vectors including the regressor samples are

$$\begin{aligned} \mathbf{U}_{\alpha 1} &= [\varphi_{\alpha 1}(5) \quad \varphi_{\alpha 1}(6) \quad \dots \quad \varphi_{\alpha 1}(N)]^T \\ \mathbf{U}_{\beta 1} &= [\varphi_{\beta 1}(5) \quad \varphi_{\beta 1}(6) \quad \dots \quad \varphi_{\beta 1}(N)]^T \\ \mathbf{U}_{\beta 2} &= [\varphi_{\beta 2}(5) \quad \varphi_{\beta 2}(6) \quad \dots \quad \varphi_{\beta 2}(N)]^T \end{aligned} \quad (16)$$

The parameter estimates $\hat{\alpha}_1$, $\hat{\beta}_1$, and $\hat{\beta}_2$ could now be computed using, e.g., the `armax` command of the System Identification Toolbox of the MATLAB software [25].¹ As a side product, the estimates \hat{c}_1 and \hat{c}_2 for the parameters of the noise polynomial are also obtained. An alternative Gauss-Newton-based algorithm [4] for parameter computation

¹Create a data object to encapsulate the input/output data and their properties: `data = iddata(Y, [U_alpha U_beta U_beta2], T_s)`. Estimate the ARMAX polynomial model using time domain data: `model = armax(data, [0 [1 1 1] 2 [0 0 0]])`.

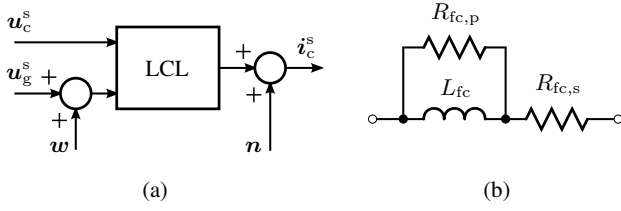


Fig. 4. (a) Simulation model of the LCL filter. Measurement noise \mathbf{n} and the grid disturbance \mathbf{w} are added. (b) Inductor model with the series and parallel resistances.

TABLE I
DATAHEET PARAMETERS AND ESTIMATED PARAMETERS FROM SIMULATIONS

Parameter	Datasheet value	Estimated parameter	Case 1	Case 2
L_{fc}	2.94 mH	\hat{L}_{fc}	2.93 mH	2.95 mH
C_f	10.0 μ F	\hat{C}_f	9.96 μ F	10.6 μ F
L_{fg}	1.96 mH	\hat{L}_{fg}	1.98 mH	1.79 mH

is presented in Appendix B. The algorithm is independent of the software and it could be implemented, e.g., in a real-time processor.

D. Continuous-Time Parameters

The continuous-time parameter estimates $\hat{\omega}_p$, \hat{L}_{fc} , and \hat{L}_{fg} can be solved from (6) as functions of the discrete-time parameter estimates $\hat{\alpha}_1$, $\hat{\beta}_1$, and $\hat{\beta}_2$:

$$\begin{aligned} \hat{\omega}_p &= \frac{1}{T_s} \arccos\left(-\frac{\hat{\alpha}_1 + 1}{2}\right) \\ \hat{L}_{fc} &= \frac{2 \frac{\sin(\hat{\omega}_p T_s)}{\hat{\omega}_p} [\cos(\hat{\omega}_p T_s) - 1]}{2\hat{\beta}_1 \left[\cos(\hat{\omega}_p T_s) - \frac{\sin(\hat{\omega}_p T_s)}{\hat{\omega}_p T_s} \right] + \hat{\beta}_2 \left[1 - \frac{\sin(\hat{\omega}_p T_s)}{\hat{\omega}_p T_s} \right]} \\ \hat{L}_{fg} &= -\frac{\hat{\omega}_p \hat{L}_{fc} [\hat{L}_{fc} \hat{\beta}_2 + 2T_s \cos(\hat{\omega}_p T_s)]}{\hat{\omega}_p \hat{L}_{fc} \hat{\beta}_2 + 2 \sin(\hat{\omega}_p T_s)} \end{aligned} \quad (17)$$

From (3), the filter capacitance becomes

$$\hat{C}_f = \frac{\hat{L}_{fc} + \hat{L}_{fg}}{\hat{\omega}_p^2 \hat{L}_{fc} \hat{L}_{fg}} \quad (18)$$

IV. RESULTS

The proposed method was evaluated by means of simulations and experiments. A 12.5-kVA grid-converter system equipped with the LCL filter is considered. The rms line-to-line grid voltage was 400 V and the grid frequency 50 Hz. The switching frequency was 6 kHz and the sampling frequency was 12 kHz. The approximate bandwidths of the DC-voltage control and the PLL were 20 Hz.

For better regulation of the operating-point currents, the current controller was augmented with an integral action,

$$\mathbf{K}(z) = k_p + \frac{T_s k_i}{z - 1} \quad (19)$$

where the proportional gain was $k_p = 1 \Omega$ and the integral gain $k_i = 0.01 \Omega/s$ was very small in order to diminish the effect of the controller on the identification.



Fig. 5. Experimental setup.

The PRBS having an amplitude of ± 32.5 V (± 0.1 p.u.) was generated using a 10-bit-length shift register. The PRBS was injected into the q-component of the voltage reference. Two periods of the PRBS were used for the identification, i.e., the number of collected samples is $N = 2046$. The parameter estimates were computed using the algorithm presented in Appendix B.

A. Simulations

Two simulation cases are considered. In Case 1, the simulation model of the LCL filter is lossless and no additional disturbances are used. The parameters of the modeled filter are given in Table I. In Case 2, the simulation model includes measurement noise, grid harmonics, and inductor losses. The measurement noise \mathbf{n} , having a standard deviation of 0.25 A (0.01 p.u.), is added according to Fig. 4(a). Further, the grid disturbance \mathbf{w} , composed of the 5th and 7th harmonics of the grid voltage, is added. Both harmonics have an amplitude of 6.5 V (0.02 p.u.). As shown in Fig. 4(b), the series resistor $R_{fc,s} = 102$ m Ω and the parallel resistor $R_{fc,p} = 420$ Ω of the converter-side inductor are included in order to model the DC resistance and the eddy-current effects. The series resistor $R_{fg,s} = 68$ m Ω and the parallel resistor $R_{fg,p} = 630$ Ω of the grid-side inductor are modeled similarly.

The simulation results are given in Table I. In Case 1, the proposed method estimates the parameters with good accuracy. In Case 2, the estimated parameters become a bit biased, mainly due to the parallel resistances and the grid harmonics. The series resistances of the inductors have only negligible effect on parameter estimates. The estimated resonance frequency $\hat{\omega}_p$ still almost equals the real value.

B. Experiments

The experiments were carried out using the setup shown in Fig. 5. It consists of two back-to-back connected 12.5-

TABLE II
EXPERIMENTALLY ESTIMATED PARAMETERS

Estimated parameter	$i_{cd} \approx 0$ A	$i_{cd} \approx 0$ A	$i_{cd} \approx 0$ A
	$i_{cq} = 5$ A	$i_{cq} = 0$ A	$i_{cq} = -5$ A
\hat{L}_{fc}	3.2 mH	3.3 mH	3.2 mH
\hat{C}_f	8.1 μ F	7.9 μ F	8.2 μ F
\hat{L}_{fg}	3.2 mH	3.2 mH	3.1 mH

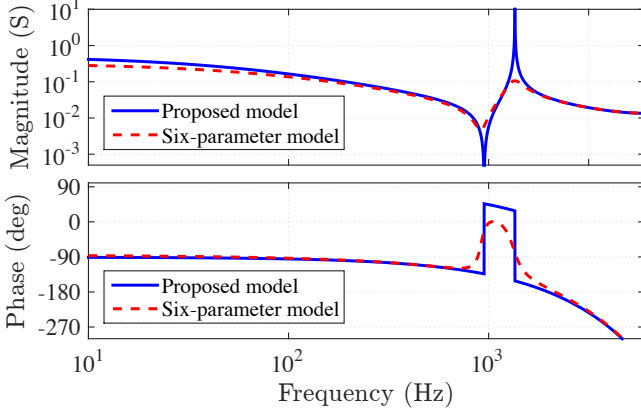


Fig. 6. Frequency responses plotted using the estimated parameters: the proposed lossless model $\mathbf{Y}(z)$ (solid blue line) and the six-parameter lossy model $\mathbf{Y}_6(z)$ (dashed red line).

kVA 50-Hz converters equipped with LCL filters. Data-sheet parameters for the LCL filters are given in Table I. An isolation transformer was used for the loading converter. Control and data acquisition of the converter under test was implemented on the dSPACE DS1006 board. The DC-bus voltage, two phase-to-phase grid voltages, and three converter phase currents were measured.

1) *Estimated Parameters:* The parameters were estimated in three operating points. In all three cases, the DC voltage was 650 V and the d-axis current i_{cd} was approximately zero in order to demonstrate a self commissioning: the converter is connected to the grid, the converter is controlling the DC-bus voltage, and no active power for the load is transmitted. The operating-point values of the q-axis currents were $i_{cq} = 5$ A, $i_{cq} = 0$ A, and $i_{cq} = -5$ A. The measurement was repeated ten times in each operating point in order to study the deviation of the parameter estimates.

Approximately 20 iteration rounds are needed for the parameters to converge to the final values. The estimated parameters $\hat{\alpha}_1$, $\hat{\beta}_1$, and $\hat{\beta}_2$ have small imaginary parts (less than 3%) compared to their real parts [theoretically $\hat{\alpha}_1$, $\hat{\beta}_1$, and $\hat{\beta}_2$ should be real according to (6)]. Table II provides the estimated values of the physical parameters. The standard deviations of the estimated physical parameters are small compared to the expected values in all operating points, i.e., less than 2% for all parameter estimates. It can also be seen that the operating point has only a modest impact on the estimates. The estimated resonance frequency $\hat{\omega}_p$ is almost the same in all operating points ($2\pi \cdot 1400$ rad/s).

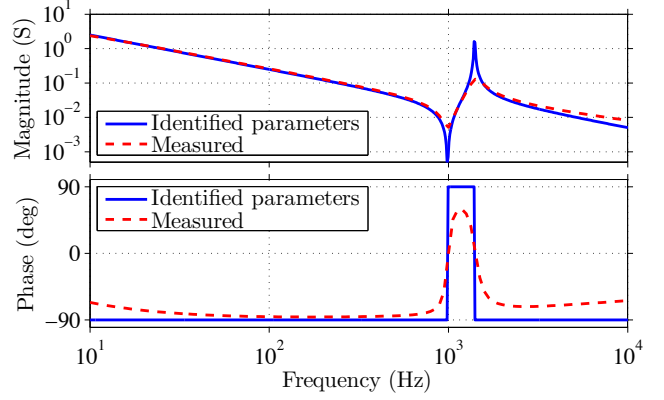


Fig. 7. Measured frequency response of the input admittance of the LCL-filter $i_c^s(j\omega)/u_c^s(j\omega)$ (dashed red line) and the calculated frequency response of the admittance using the estimated parameters (solid blue line).

2) *Comparison With a Lossy Model:* The proposed lossless model (5) is constructed using the estimated parameter values ($\hat{L}_{fc} = 3.2$ mH, $\hat{C}_f = 8.1$ μ F, $\hat{L}_{fg} = 3.2$ mH). Further, a more general six-parameter lossy model is estimated:

$$\mathbf{Y}_6(z) = z^{-1} \frac{\mathbf{b}_1 z^{-1} + \mathbf{b}_2 z^{-2} + \mathbf{b}_3 z^{-3}}{1 + \mathbf{a}_1 z^{-1} + \mathbf{a}_2 z^{-2} + \mathbf{a}_3 z^{-3}} \quad (20)$$

where $\mathbf{a}_1 \dots \mathbf{a}_3$ and $\mathbf{b}_1 \dots \mathbf{b}_3$ are independent parameters. Fig. 6 shows the estimated frequency responses for both the proposed model and for the six-parameter model in synchronous coordinates. As can be seen, the frequency responses resemble each other below the antiresonance frequency and above the resonance frequency. The resonance frequency is $2\pi \cdot 1350$ rad/s for the six-parameter model and $2\pi \cdot 1350$ rad/s for the proposed model. The antiresonance frequency is $2\pi \cdot 950$ rad/s for the six-parameter model and $2\pi \cdot 910$ rad/s for the proposed model. This indicates that the lossless model of the LCL filter is sufficient for control purposes.

3) *Validation in Frequency Domain:* The estimation result is validated in the frequency domain. The frequency response of the converter-side input admittance, $i_c^s(j\omega)/u_c^s(j\omega)$, cf. Fig. 1, of the LCL filter was measured with the frequency-response analyzer NF FRA5097 when the grid-side terminals of the filter were short circuited. The measured response is compared with the calculated frequency response for the lossless filter using the estimated parameter values ($\hat{L}_{fc} = 3.2$ mH, $\hat{C}_f = 8.1$ μ F, $\hat{L}_{fg} = 3.2$ mH). Fig. 7 shows the measured and calculated responses in stator coordinates. As the figure shows, the calculated frequency response match well with the measured response, i.e., the estimated lossless model predicts well the resonance and the anti-resonance frequencies as well as the slopes at high and low frequencies.

4) *Comparison in Controller Tuning:* A two-degree-of-freedom (2DOF) state-feedback current controller [3] was tuned using the datasheet parameter values given in Table I and the estimated parameter values ($\hat{L}_{fc} = 3.2$ mH, $\hat{C}_f = 8.1$ μ F, $\hat{L}_{fg} = 3.2$ mH). The closed-loop dominant dynamics for the current-reference tracking were specified to correspond to the

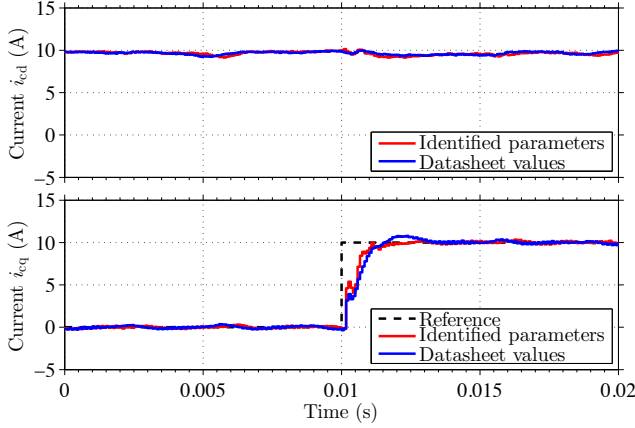


Fig. 8. Measured waveforms of the d (above) and q (below) current components when the 2DOF state-feedback controller is tuned using the datasheet parameter values and the identified parameter values.

first-order system with the bandwidth of 600 Hz. Fig. 8 shows the measured waveforms of the converter current components in synchronous coordinates, when the q-axis current reference steps from zero to 10 A at $t = 0.01$ s. During the step the converter was supplying the power of 5 kW to the grid yielding $i_{cd} = 10$ A. As the figure shows, the step response corresponds well the designed dynamics (5-% settling time is 1 ms and there is no overshoot) when the identified parameters are used. This indicates that the estimated values are more accurate from the controller point of view in comparison with the data-sheet values.

V. CONCLUSION

This paper proposes a method to identify the discrete-time transfer-function parameters and the corresponding physical parameters of an LCL filter from a controller point of view. The physical parameters were obtained by comparing the estimated discrete-time model with the analytical discrete-time model. According to the simulation and experimental results, the proposed method can be used to find the physical parameter values of the LCL filter. A control system of the grid converters is typically based on the lossless model of an LCL filter. Since the proposed method estimates the desired parameters of the lossless model directly, the method enables self-commissioning of a grid converter.

APPENDIX A DISCRETE-TIME MODEL

A discrete-time model of the lossless LCL filter in synchronous coordinates is presented in the following. The PWM is modeled as the zero-order hold (ZOH) in stationary coordinates. The sampling of the converter currents and the grid voltages are synchronized with the PWM. Under these assumptions, the hold-equivalent discrete-time state-space model

of the LCL filter becomes [3]

$$\begin{aligned} \mathbf{x}(k+1) &= \mathbf{A}\mathbf{x}(k) + \mathbf{B}_c\mathbf{u}_c(k) + \mathbf{B}_g\mathbf{u}_g(k) \\ \mathbf{i}_c(k) &= \mathbf{C}\mathbf{x}(k) \end{aligned} \quad (21)$$

where the state vector is selected as $\mathbf{x} = [\mathbf{i}_c, \mathbf{u}_f, \mathbf{i}_g]^T$. The system matrices are

$$\begin{aligned} \mathbf{A} &= \gamma \begin{bmatrix} L_{fc} + L_{fg} \cos(\omega_p T_s) & -\frac{\sin(\omega_p T_s)}{\omega_p L_{fc}} & \frac{L_{fg}[1 - \cos(\omega_p T_s)]}{L_t} \\ \frac{\sin(\omega_p T_s)}{\omega_p C_f} & \cos(\omega_p T_s) & -\frac{\sin(\omega_p T_s)}{\omega_p C_f} \\ \frac{L_{fc}[1 - \cos(\omega_p T_s)]}{L_t} & \frac{\sin(\omega_p T_s)}{\omega_p L_{fg}} & \frac{L_{fg} + L_{fc} \cos(\omega_p T_s)}{L_t} \end{bmatrix} \\ \mathbf{B}_c &= \frac{\gamma}{L_t} \begin{bmatrix} T_s + \frac{L_{fg} \sin(\omega_p T_s)}{\omega_p L_{fc}} \\ L_{fg}[1 - \cos(\omega_p T_s)] \\ T_s - \frac{\sin(\omega_p T_s)}{\omega_p} \end{bmatrix}, \quad \mathbf{C} = [1 \ 0 \ 0] \end{aligned} \quad (22)$$

The closed-form expression for the input matrix \mathbf{B}_g in (21) can be found in [3].

The converter current $\mathbf{i}_c(k)$ can be solved as

$$\begin{aligned} \mathbf{i}_c(k) &= \mathbf{C}(z\mathbf{I} - \mathbf{A})^{-1}\mathbf{B}_c\mathbf{u}_c(k) \\ &= \frac{\beta_1\gamma z^{-1} + \beta_2\gamma^2 z^{-2} + \beta_3\gamma^3 z^{-3}}{1 + \alpha_1\gamma z^{-1} - \alpha_2\gamma^2 z^{-2} + \gamma^3 z^{-3}}\mathbf{u}_c(k) \end{aligned} \quad (23)$$

where the parameters α_1 , β_1 , and β_2 are given in (6). The actual converter voltage \mathbf{u}_c is produced based on the voltage reference $\mathbf{u}_{c,\text{ref}}$. Due to the finite computational time of the control algorithm, the converter-voltage reference calculated at the present time step becomes active at the next time step

$$\mathbf{u}_c(k) = z^{-1}\mathbf{u}_{c,\text{ref}}(k) \quad (24)$$

where the angular compensation is assumed to be embedded in the coordinate transformation according to Fig. 2(a). Combining (23) and (24) gives the pulse-transfer operator in (5).

APPENDIX B PARAMETER COMPUTATION ALGORITHM

The predictor $\hat{\mathbf{y}}(k)$ can be constructed by taking the expected value of \mathbf{y} in (12), yielding

$$\begin{aligned} \hat{\mathbf{y}}(k) &= \left(1 - \frac{1}{\mathbf{C}(z)}\right)\mathbf{y}(k) \\ &+ \frac{1}{\mathbf{C}(z)}[\alpha_1\boldsymbol{\varphi}_{\alpha_1}(k) + \beta_1\boldsymbol{\varphi}_{\beta_1}(k) + \beta_2\boldsymbol{\varphi}_{\beta_2}(k)] \end{aligned} \quad (25)$$

The prediction error

$$\begin{aligned} \boldsymbol{\varepsilon}(k) &= \mathbf{y}(k) - \hat{\mathbf{y}}(k) \\ &= \frac{1}{\mathbf{C}(z)}[\mathbf{y}(k) - \alpha_1\boldsymbol{\varphi}_{\alpha_1}(k) - \beta_1\boldsymbol{\varphi}_{\beta_1}(k) - \beta_2\boldsymbol{\varphi}_{\beta_2}(k)] \end{aligned} \quad (26)$$

describes the part that cannot be predicted with the model. The aim is to find the parameter vector

$$\hat{\boldsymbol{\theta}} = [\hat{\alpha}_1 \ \hat{\beta}_1 \ \hat{\beta}_2 \ \hat{c}_1 \ \hat{c}_2] \quad (27)$$

that minimizes the prediction errors.

The parameter computation is a three-stage procedure having the following order: 1) the ordinary least squares (OLS) method; 2) the iterative extended least squares (ELS) method;

and 3) the iterative Gauss-Newton method. The ELS method gives the first estimate of $\hat{\theta}$ for the Gauss-Newton algorithm. Further, the ELS method requires some knowledge about the prediction errors, for which the OLS method is performed first.

Before computation, the regressor vectors $\mathbf{U}_{\alpha 1}$, $\mathbf{U}_{\beta 1}$, $\mathbf{U}_{\beta 2}$ and the output vector \mathbf{Y} are constructed as described in Section III-C. The computation starts from the OLS stage, where the autoregressive with exogenous input (ARX) model structure is assumed, i.e., $\hat{c}_1 = \hat{c}_2 = 0$. The parameter vector $\hat{\theta}_{\text{ARX}} = [\hat{\alpha}_1, \hat{\beta}_1, \hat{\beta}_2]^T$ is solved as [4]

$$\hat{\theta}_{\text{ARX}} = (\Phi_{\text{ARX}}^H \Phi_{\text{ARX}})^{-1} \Phi_{\text{ARX}}^H \mathbf{Y} \quad (28)$$

where $\Phi_{\text{ARX}} = [\mathbf{U}_{\alpha 1}, \mathbf{U}_{\beta 1}, \mathbf{U}_{\beta 2}]$ is the regressor matrix for the ARX model and the conjugate transpose is marked with H.

In the following stages, the ARMAX-model structure is used. Using the ELS method, the parameter vector $\hat{\theta}$ is solved iteratively:

$$\hat{\theta}_{v+1} = (\Phi_v^H \Phi_v)^{-1} \Phi_v^H \mathbf{Y} \quad (29)$$

where v is the iteration round. The regressor matrix Φ is extended with delayed prediction-error vectors \mathbf{E} :

$$\Phi_v = [\mathbf{U}_{\alpha 1} \quad \mathbf{U}_{\beta 1} \quad \mathbf{U}_{\beta 2} \quad z^{-1}\mathbf{E}_v \quad z^{-2}\mathbf{E}_v] \quad (30)$$

The prediction-error vector $\mathbf{E} = [\varepsilon(5), \varepsilon(6) \dots \varepsilon(N)]^T$ is solved using (26) in each iteration round:

$$\mathbf{E}_v = \frac{1}{\hat{C}_v(z)} \left(\mathbf{Y} - \hat{\alpha}_{1,v} \mathbf{U}_{\alpha 1} - \hat{\beta}_{1,v} \mathbf{U}_{\beta 1} - \hat{\beta}_{2,v} \mathbf{U}_{\beta 2} \right) \quad (31)$$

In the first round, we can use the prediction-error vector obtained in the OLS stage. Iterations are continued, until the parameter estimate $\hat{\theta}$ can be applied in the Gauss-Newton algorithm.

Finally, the Gauss-Newton algorithm is performed. The parameter vector $\hat{\theta}$ is solved iteratively, starting from the initial value of $\hat{\theta}$ obtained in the ELS stage:

$$\hat{\theta}_{v+1} = \hat{\theta}_v - (\mathbf{J}_v^H \mathbf{J}_v)^{-1} \mathbf{J}_v^H \mathbf{E}_v \quad (32)$$

The Jacobian matrix \mathbf{J} of the prediction-error vector \mathbf{E} is expressed as

$$\mathbf{J}_v = \frac{\partial \mathbf{E}_v}{\partial \hat{\theta}_v} = - \frac{1}{\hat{C}_v(z)} \Phi_v \quad (33)$$

Iterations are continued until the estimated parameters converge to the final values.

ACKNOWLEDGMENT

The authors gratefully acknowledge ABB Oy and Walter Ahlström Foundation for the financial support.

REFERENCES

- [1] S. Mariéthoz and M. Morari, "Explicit model-predictive control of a PWM inverter with an LCL filter," *IEEE Transactions on Industrial Electronics*, vol. 56, no. 2, pp. 389–399, Feb. 2009.
- [2] J. Dannehl, F. W. Fuchs, and P. B. Thøgersen, "PI state space current control of grid-connected PWM converters with LCL filters," *IEEE Transactions on Power Electronics*, vol. 25, no. 9, pp. 2320–2330, Sept. 2010.
- [3] J. Kukkola, M. Hinkkanen, and K. Zenger, "Observer-based state-space current controller for a grid converter equipped with an LCL filter: Analytical method for direct discrete-time design in synchronous coordinates," in *IEEE Energy Conversion Congress and Exposition (ECCE)*, Pittsburgh, PA, Sept. 2014, pp. 4458–4465.
- [4] L. Ljung, *System Identification: Theory for the User*, 2nd ed. Troy, NY: Prentice-Hall, 1999.
- [5] J. Rhode, A. Kelley, and M. Baran, "Complete characterization of utilization-voltage power system impedance using wideband measurement," *IEEE Transactions on Industry Applications*, vol. 33, no. 6, pp. 1472–1479, Nov. 1997.
- [6] M. Liserre, F. Blaabjerg, and R. Teodorescu, "Grid impedance estimation via excitation of LCL-filter resonance," *IEEE Transactions on Industry Applications*, vol. 43, no. 5, pp. 1401–1407, Sept. 2007.
- [7] N. Hoffmann and F. Fuchs, "Minimal invasive equivalent grid impedance estimation in inductive-resistive power networks using extended Kalman filter," *IEEE Transactions on Power Electronics*, vol. 29, no. 2, pp. 631–641, Feb. 2014.
- [8] D. Reigosa, F. Briz, C. Charro, P. Garcia, and J. Guerrero, "Active islanding detection using high-frequency signal injection," *IEEE Transactions on Industry Applications*, vol. 48, no. 5, pp. 1588–1597, Sept. 2012.
- [9] L. Asiminoaei, R. Teodorescu, F. Blaabjerg, and U. Borup, "Implementation and test of an online embedded grid impedance estimation technique for PV inverters," *IEEE Transactions on Industrial Electronics*, vol. 52, no. 4, pp. 1136–1144, Aug. 2005.
- [10] M. Cespedes and J. Sun, "Adaptive control of grid-connected inverters based on online grid impedance measurements," *IEEE Transactions on Sustainable Energy*, vol. 5, no. 2, pp. 516–523, Apr. 2014.
- [11] S. Cobrecas, E. Bueno, D. Pizarro, F. Rodriguez, and F. Huerta, "Grid impedance monitoring system for distributed power generation electronic interfaces," *IEEE Transactions on Instrumentation and Measurement*, vol. 58, no. 9, pp. 3112–3121, Sept. 2009.
- [12] M. Sumner, A. Abusorrah, D. Thomas, and P. Zanchetta, "Real time parameter estimation for power quality control and intelligent protection of grid-connected power electronic converters," *IEEE Transactions on Smart Grid*, vol. 5, no. 4, pp. 1602–1607, July 2014.
- [13] P. Garcia, J. Guerrero, J. Garcia, A. Navarro-Rodriguez, and M. Sumner, "Low frequency signal injection for grid impedance estimation in three phase systems," in *Energy Conversion Congress and Exposition (ECCE)*, Pittsburgh, PA, Sept. 2014, pp. 1542–1549.
- [14] T. Roinila, M. Vilkkko, and J. Sun, "Online grid impedance measurement using discrete-interval binary sequence injection," *IEEE Journal of Emerging and Selected Topics in Power Electronics*, vol. 2, no. 4, pp. 985–993, Dec. 2014.
- [15] D. Martin and E. Santi, "Autotuning of digital deadbeat current controllers for grid-tie inverters using wide bandwidth impedance identification," *IEEE Transactions on Industry Applications*, vol. 50, no. 1, pp. 441–451, Jan. 2014.
- [16] K.-W. Lee, M. Kim, J. Yoon, K.-W. Lee, and J.-Y. Yoo, "Condition monitoring of dc-link electrolytic capacitors in adjustable-speed drives," *IEEE Transactions on Industry Applications*, vol. 44, no. 5, pp. 1606–1613, Sept. 2008.
- [17] F. Huerta, S. Cobrecas, F. Rodriguez, D. Pizarro, and F. Meca, "Black-box identification for an auto-tuned current controller working with voltage source converters connected to the grid through a LCL filter," in *IEEE International Symposium on Industrial Electronics (ISIE)*, Bari, Italy, July 2010, pp. 96–101.
- [18] F. Huerta, S. Cobrecas, F. Rodriguez, C. Clancey, and I. Sanz, "Comparison of two black-box model identification methods applied on a VSC with LCL filter," in *38th Annual Conference of IEEE Industrial Electronics Society*, Montreal, Canada, Oct. 2012, pp. 4648–4653.
- [19] J. Massing, M. Stefanello, H. Grundling, and H. Pinheiro, "Adaptive current control for grid-connected converters with LCL filter," *IEEE Transactions on Industrial Electronics*, vol. 59, no. 12, pp. 4681–4693, Dec. 2012.

- [20] R. Peña Alzola, M. Liserre, F. Blaabjerg, M. Ordonez, and T. Kerekes, "A self-commissioning notch filter for active damping in a three-phase LCL-filter-based grid-tie converter," *IEEE Transactions on Power Electronics*, vol. 29, no. 12, pp. 6754–6761, Dec. 2014.
- [21] S. Gomez Jorge, C. Busada, and J. Solsona, "Frequency-adaptive current controller for three-phase grid-connected converters," *IEEE Transactions on Industrial Electronics*, vol. 60, no. 10, pp. 4169–4177, Oct. 2013.
- [22] K. Jalili and S. Bernet, "Design of LCL filters of active-front-end two-level voltage-source converters," *IEEE Transactions on Industrial Electronics*, vol. 56, no. 5, pp. 1674–1689, May 2009.
- [23] U. Forssell and L. Ljung, "Closed-loop identification revisited," *Automatica*, vol. 35, pp. 1215–1241, July 1999.
- [24] H. Garnier, "Data-based continuous-time modelling of dynamic systems," in *International Symposium on Advanced Control of Industrial Processes (ADCONIP)*, Hangzhou, China, May 2011, pp. 146–153.
- [25] L. Ljung, *System Identification Toolbox: User's Guide*, Mathworks, Natick, MA, 2014.